Biosensors and Bioelectronics 290 (2025) 117992

Contents lists available at ScienceDirect

Biosensors and Bioelectronics

journal homepage: www.elsevier.com/locate/bios

Potential-pulse-assisted co-immobilization of multiple aptamers on microelectrode arrays for multiplexed neurotransmitter detection

Ziheng Hu [a,b], Ruifeng Zhu [a], Gabriela Figueroa-Miranda [a], Lingyan Feng [c], Andreas Offenhäusser [a], Dirk Mayer [a,*]

[a] Institute of Biological Information Processing, Bioelectronics (IBI-3), Forschungszentrum Jülich GmbH, 52428, Jülich, Germany
[b] Faculty I, RWTH Aachen University, 52062, Aachen, Germany
[c] Materials Genome Institute, Shanghai University, 200444, Shanghai, China

A B S T R A C T

Accurate and simultaneous determination of multiple neurotransmitters (NTs) is crucial for a thorough understanding of brain functions and for diagnosing neurological disorders. We have developed an electrochemical biosensor utilizing aptamer recognition for the highly sensitive and simultaneous detection of multiple neurotransmitters, including glutamate quantification for the first time in multiplex detection. Microelectrode arrays (MEAs) served as biosensing platforms to facilitate the recording of signals from multiple channels, rapid mass transfer rates, and high spatial resolution, fundamental for studying NTs release in nervous tissue. To enhance aptamer receptor loading, gold nanostructures were electrodeposited onto the microelectrodes, enhancing the active surface area and electrode morphology. A potential-pulse-assisted method was employed to achieve site-selective immobilization of three different aptamers on a single MEA chip within 30 min, enabling fast and reproducible sensor fabrication. This unique strategy ensured aptamer-specific immobilization, minimized cross-talk, and allowed for multiplex detection of serotonin, glutamate, and dopamine with high sensitivity and specificity. Additionally, using polyethylene glycol (PEG) as a blocking molecule, the aptamer-functionalized MEAs showed enhanced antifouling properties and maintained detection capabilities in complex environments. This multiplexed detection strategy enables a high-performance and robust biosensor platform with strong clinical relevance, offering substantial potential for *in vivo* monitoring of neurotransmitter release and the diagnosis of neurological disorders.

1. Introduction

Neurotransmitters (NTs) are neurochemicals that play a pivotal role in neuronal signal transmission across the central nervous system (CNS) (Zhang et al., 2021). Dysregulation of NTs is implicated in numerous mental disorders, such as Alzheimer's disease (AD) and depression. Accurate and simultaneous detection of NTs levels holds significant promise for clinical diagnosis and therapeutic interventions (Pradhan et al., 2014). Moreover, monitoring the real-time release and dynamic interplay between various NTs in different brain regions may provide a comprehensive understanding of brain functions in regulating complex physiological and biological processes (Teleanu et al., 2022). Conventional techniques for NTs detection such as microdialysis, high-performance liquid chromatography (HPLC), and mass spectrometry (MS) are limited by disadvantages of time-consuming procedures, the need for sophisticated instrumentation, and high costs (Ma et al., 2020; Wojnicz et al., 2016). Electrochemical methods offer a simple, fast, and highly sensitive alternative for NTs detection (Bucher and Wightman, 2015). Fast-scan cyclic voltammetry (FSCV) is a powerful electrochemical technique used for the real-time detection of NT release, enabled by the recording of electrochemical signals associated with NTs oxidation and reduction (Venton and Cao, 2020). However, many NTs have similar oxidation potentials, making it difficult to distinguish between them due to overlapping redox responses. Additionally, the detection of non-electroactive NTs requires their conversion by enzymes, which presents challenges related to spatial resolution and invasiveness (Arumugasamy et al., 2020). Therefore, further advancements are required to develop highly specific bioreceptors for NTs determination.

Aptamers, which are mostly short single-stranded (ss) DNA or RNA molecules, have emerged as versatile bioreceptors for recognizing small molecules with inherent high specificity. Isolating via the systematic evolution of ligands by exponential enrichment (SELEX) process, aptamers offer distinct advantages compared to antibodies, such as cost-effective chemical synthesis, enhanced thermal stability, and facile modification with functional groups (Yu et al., 2021). To date, various aptamers targeting selected NTs, including glutamate (Glu), dopamine (DA), and serotonin (ST), have been reported (Moraldo et al., 2022;

* Corresponding author
E-mail address: dirk.mayer@fz-juelich.de (D. Mayer).

https://doi.org/10.1016/j.bios.2025.117992
Received 22 June 2025; Received in revised form 7 September 2025; Accepted 11 September 2025
Available online 13 September 2025

Nakatsuka et al., 2018; Wu et al., 2022). Consequently, diverse biosensor platforms utilizing aptamers as receptors have been deployed for NTs detection, providing significant advancements in neurochemical detection methodologies (Hu et al., 2023a). Among these, electrochemical aptamer-based (E-AB) sensors enable sensitive, simple, and rapid sensing of NTs, while miniaturization holds great potential for point-of-care, *in vivo*, and clinical applications (Downs and Plaxco, 2022). Typically, an E-AB sensor consists of an electrode surface functionalized with aptamers specific to the analyte. Sensor signals arise through the target-binding events, leading to conformational changes in the surface-tethered aptamers altering the structural and chemical composition of the electrochemical double layer. Various electrochemical investigation methods can be utilized to monitor these changes and link the resulting signal to the concentration of the analyte (Wu et al., 2020).

Current E-AB sensors are predominantly capable of detecting only one target at a time, unable to multiplex the analyte detection (Negahdary and Angnes, 2022). However, the measurement of various analytes from the same sample can undoubtedly improve the diagnostics and help to understand complex biological processes such as information processing in neuronal networks as it provides more information about the system under study than when only a single analyte is measured (Sen and Lazenby, 2024). One straightforward strategy for the detection of multiple targets involves the incorporation of several types of aptamers each with unique redox probes all on a single electrode (Hansen et al., 2006; Ma et al., 2018). However, electrodes modified with diverse aptamers lack spatiotemporal resolution and suffer from interferences during multiplex target sensing. Furthermore, all aptamers have to share the same electrode reducing the number of the individual receptors, which leads to decreased signal intensity for each analyte. Additionally, each aptamer requires a unique packing density to facilitate the optimal target binding which cannot be established via this immobilization method (Li et al., 2018; Shen et al., 2021). An alternative approach for multiplexed sensing utilizes multielectrode arrays (MEAs) with spatially separated electrodes, enabling recording of concurrent signals occurring across different sections of the array (Torrente-Rodríguez et al., 2020). The integration of distinct bioreceptors on individual electrodes enables the generation of distinguishable signals in each channel of the MEA. In comparison with the utilization of individual electrodes in separate wells, the MEAs platform facilitates simultaneous multi-analyte detection within a single sample, thereby eradicating well-to-well variability, facilitating easier calibration and enhancing the detection reproducibility. Additionally, this approach significantly reduces the required sample volume, enables compact and portable devices making it particularly valuable for clinical and *in vivo* studies. The platform's ability to perform spatially resolved detection allows for the monitoring of spatiotemporal variations of the level of several analytes, which is of critical importance in neuroscience and biomedical research (Munge et al., 2016; Sharafeldin and Rusling, 2023; Timilsina et al., 2021). Knowing for instance the local concentrations of several NTs at a given time provide deeper insights into the complex events during signal processing within the brain. Analyzing various chemical messengers such as DA, ST, and Glu enables a deeper understanding on how the balance between excitatory and inhibitory signals is established, which is responsible for all cognitive processes. Additionally, different brain regions often display characteristic chemical profiles. A detailed understanding of regional NT concentrations allows to examine specific neural networks more precisely, shedding light on which areas are active and how they interact with each other (Teleanu et al., 2022). The usefulness of multi-analyte detection by a single sensor chip was demonstrated by our group previously already by establishing an E-AB sensor on flexible-MEAs for the simultaneous detection of two diabetes biomarkers as well as for the detection of two malaria biomarkers by four different aptamer receptors (Figueroa-Miranda et al., 2021; Zhou et al., 2023).

A general challenge in the development of multi-analyte sensors is the immobilization of the corresponding multiple aptamers on the different individual electrodes of the MEAs. One direct but technologically demanding method is the selective spotting of solution droplets containing a specific bioreceptor onto individual electrodes (Song et al., 2014). However, this method is not well suited for MEAs with minimal intra-electrode spacing due to the potential spreading of the solution from one electrode to adjacent ones. Furthermore, electrochemical striping of adsorbed aptamers from selected electrodes and consecutive immobilization of different aptamers can be used, but this process is time-consuming (Zhang et al., 2020). Electrochemical grafting via diazonium chemistry can selectively modify receptors on closely spaced microelectrodes within an array through electrochemical deposition (Fan et al., 2020; Feng et al., 2016). Although it provides a low-cost method for specific electrode modification, the necessity of pre-treatment for surface functionalization with linker groups complicates the process (Gao et al., 2022). Another promising approach is the use of electric field-assisted grafting of DNA probes by controlling the electrode potential, which allows for the production of different self-assembled monolayers on neighboring gold electrodes (Jambrec and Gebala, 2022; Veselinovic et al., 2018). For instance, a positive potential can attract negatively charged DNA close to the electrode surface, facilitating its immobilization, while a negative potential repels DNA strands, moving them into an upright orientation and creating space for new strands to approach the surface (Ge et al., 2003; Gibson and Mendes, 2021). Jambrec et al. integrated this electric field-assisted method with pulse-type potential modulation and achieved highly reproducible and rapid immobilization of ssDNA on gold surfaces (Jambrec et al., 2015). By quickly switching between positive and negative potentials, the proposed potential-pulse-assisted deposition can accelerate the DNA transport from the bulk solution to the electrode surface. Meanwhile, diverse probes of interest can be site-selectively introduced to the vacated surface by controlling the circuit switch on the desired electrode (Jambrec et al., 2019).

In this study, the development of a multiple aptamer-functionalized gold MEAs chip is described for the simultaneous detection of various NTs. To enlarge the active surface areas and enhance sensor performance, a 3-dimensional (3D) nanostructured surface was introduced on the microelectrodes via gold electrodeposition (AuED) (Soleymani et al., 2009). Subsequently, a potential-pulse-assisted (PA) method was employed to achieve a site-selective immobilization of multiple aptamers on designated electrodes of the microelectrode array. Unlike conventional passive drop-casting, this approach significantly accelerates immobilization process by rapidly switching the applied potentials, which generates a local "stirring effect" that drives aptamer molecules toward the electrode surface and enhances their binding efficiency. This strategy not only reduces the overall functionalization time from many hours to approximately 30 min but also enables precise spatial control of receptor placement, ensuring reproducible and high-performance sensor fabrication. After cleaning, the ST-aptamer was first modified by PA deposition on a set of preselected microelectrodes in AuED-MEAs chip, following with thiol-PEG blocking. For multiple aptamer modifications, adjacent microelectrodes without ST-aptamer modifications were used. The microelectrodes selected for the second aptamer were cleaned to induce a desorption of adsorbed thiol molecules. After electrochemical cleaning, these microelectrodes were modified with the Glu-aptamer and thiol-PEG using the same PA procedure. This entire process of reconnecting electrodes, desorbing falsely-adsorbed aptamers, and adsorbing a new DA-aptamer monolayer was repeated for a third set of microelectrodes (Fig. 1). When the tested analytes bind to the receptors, the conformational change in the aptamers rearranges the location of the redox tag at the terminal ends, altering the electron transfer rate and leading to variations in the detectable current signals. As a result, the platform achieves simultaneous detection of ST, Glu, and DA, with Glu quantification being demonstrated in a multiplex format for the first time.

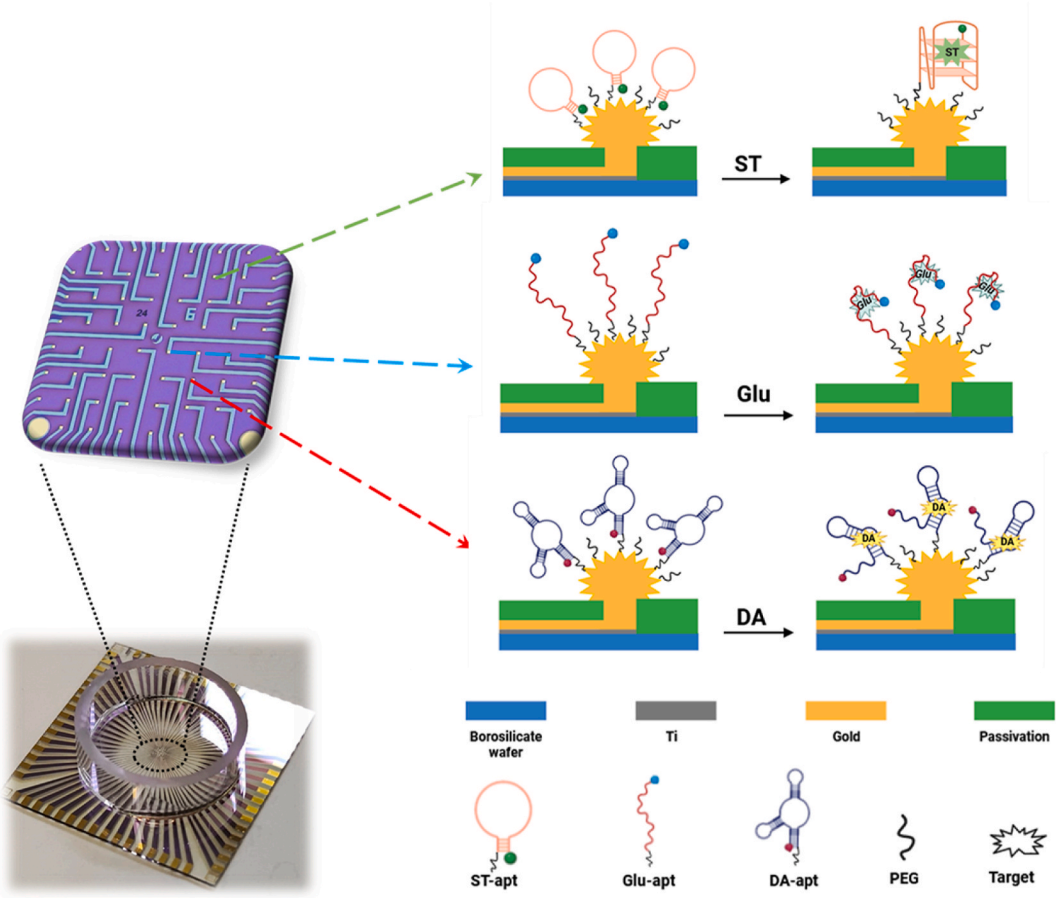

Fig. 1. An image of the MEA chip with glass ring (bottom left). Schematic illustration of the multiplexed electrochemical aptasensor for simultaneous detection of serotonin, glutamate, and dopamine. The different aptamer receptors are immobilized on separate electrodes modified with nanogold, such that each individual electrode detects a corresponding analyte. Aptamer specific redox tags further support the high specificity of the multianalyte detection. The addition of the target induces conformational changes in the respective aptamer, leading to variations in the detectable current signals.

2. Experimental section

The used HPLC-purified aptamers were obtained from FRIZ Biochem (Neuried, Germany). The detailed sequences were as follows:

Truncated serotonin aptamer (ST-apt, $K_d = 30$ nM) (Hu et al., 2023b; Nakatsuka et al., 2018): 5′-OH-$(CH_2)_6$-S-S-$(CH_2)_6$-TAG GCA GAT AGG GGA AGC TGA TTC GAT GCG TG-MB- 3′

Glutamate aptamer (Glu-apt, $K_d = 12$ μM) (Wu et al., 2022): 5′-OH-$(CH_2)_6$-S-S-$(CH_2)_6$ -GCA TCA GTC CAC TCG TGA GGT CGA CTG ATG AGG CTC GAT-Fc- 3′

Dopamine aptamer (DA-apt, $K_d = 44$ μM) (Liu et al., 2021): 5′-OH-$(CH_2)_6$-S-S-$(CH_2)_6$ -ACG CCA GTT TGA AGG TTC GTT CGC AGG TGT GGA GTG ACG T-AQ- 3′

The aptamer concentrations were determined by recording the absorbance at a 260 nm wavelength with UV/vis spectroscopy. Other reagents, apparatus and methods used in this work were described in Supplementary Material.

3. Results and discussion

3.1. Potential pulse-assisted receptor-layer immobilization

AuED-MEAs were fabricated according to an optimized protocol and used for E-AB sensor platform (see Supplementary Material, Fig. S1–S4). To achieve rapid immobilization kinetics and optimal aptamer coverage, the PA method was employed with potential-pulse modulation on the electrode. When the potential is shifted to positive values relative to the pzc, anions are driven towards the electrode surface while cations migrate towards the bulk solution (Jambrec et al., 2015). Additionally, a fraction of the cations surrounding the DNA near the electrode experience a repulsion force, thereby reducing the charge screening around the DNA strands (Tomić et al., 2007). Consequently, parts of the DNA are drawn towards the surface, subsequently pulling the strands closer to the electrode. This sequential attraction gradually aligns the entire DNA strand flat on the electrode surface. Conversely, negative potentials repel DNA strands near the electrode together with buffer anions, inducing an upright orientation of the strands. Quick switching between positive and negative potentials drives a stirring motion, effectively trapping additional DNA strands from the bulk solution and accelerating the immobilization process (Fig. 2, top). Therefore, the pzc values of the AuED-MEAs were determined in the solution for aptamer immobilization. According to the Gouy-Chapman-Stern model of the electrochemical double layer, the differential capacitance (C_d) reaches a minimal value when the potential approaches the pzc value at low ionic strength (Ter-Ovanessian et al., 2014). From plotting C_d as a function of the applied potential, the pzc for AuED-MEAs was determined to be 0.43 ± 0.03 V. After aptamer immobilization, this value shifted towards more negative potentials due to the DNA associated phosphate groups tethered to the electrode surface, resulting in a pzc (Apt/AuED-MEAs) of 0.24 ± 0.04 V (Fig. 2, bottom). It is crucial to consider this shift of pzc values when defining the optimal potentials for the immobilization of aptamers.

To achieve a high aptamer immobilization efficiency and surface

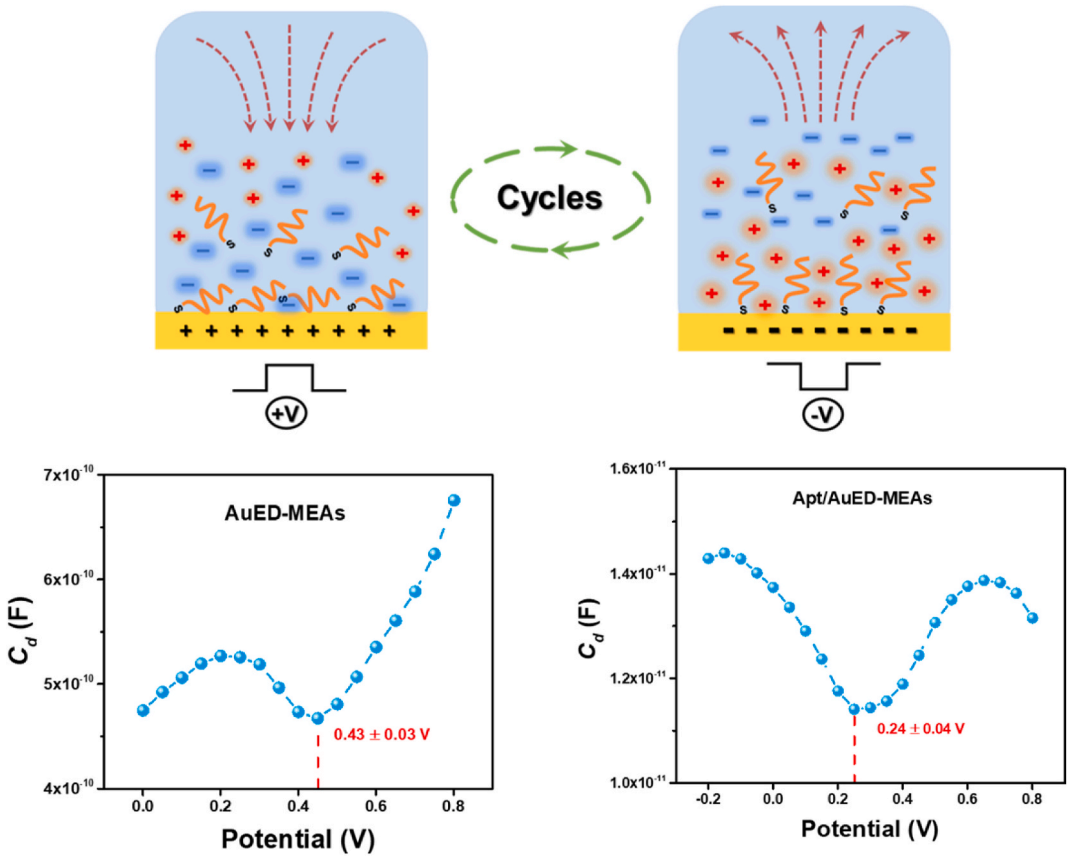

Fig. 2. Pulse-assisted immobilization of the ssDNA aptamer molecules on the electrode surface. Arrows indicate the migration directions of aptamers between the electrode and bulk solution (top). Interfacial capacitance (C_d) as a function of applied potential (V) for AuED-MEAs and aptamer modified AuED-MEAs/Apt. The potential of zero charge (pzc) value is determined at the minimum of C_d, indicated by the red dashed line (bottom).

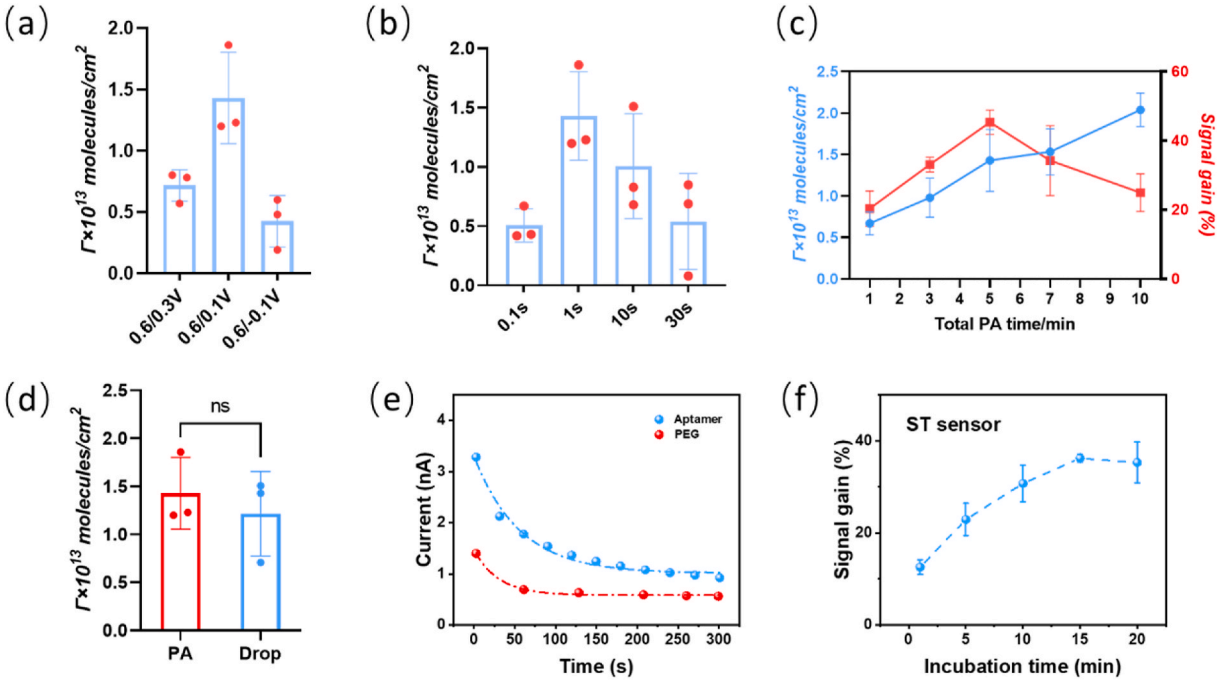

Fig. 3. Effect of the applied potential (a) and pulse duration (b) on the immobilization efficiency of pulse-assisted aptamer deposition. (c) Effect of the total pulse-assisted deposition time on the ST aptamer immobilization efficiency and the associated signal gain. (d) Comparison of aptamer immobilization by the PA (red) and drop casting (blue) method (ns: no significance). (e) *I-t* curve of aptamer and PEG immobilization on AuED-MEAs during PA molecule deposition. (f) Optimization of the incubation time for ST aptasensor after the addition of 10 nM ST.

coverage, the pulse profiles of the PA deposition procedure were thoroughly investigated using the ST-aptamer as a model receptor. Generally, the pulse potential must significantly exceed the pzc of the modified electrode surface to ensure an abundance of positive charges at the electrode interface. Simultaneously, it is imperative to maintain the active pulse potential below the onset potential for gold-sulfur bond oxidation. To illustrate the importance of selecting suitable immobilization potentials with a sufficient pulse magnitude, we compared three potential-pulse profiles using a consistent upper potential (+0.6 V) and 1 s pulse duration with varying lower potentials (Fig. 3a). The pulse profile of +0.6/+0.1 V, which possesses a positive upper potential with respect to the pzc of both AuED-MEAs and Apt/AuED-MEAs and a negative lower potential with respect to the respective pzc's, yielded the highest surface coverage, indicating the best immobilization efficiency for the applied potential-pulse sequences. In contrast, when both potentials were positive to the pzc of the Apt/AuED-MEAs using a pulse profile of +0.6/+0.3 V, the immobilized aptamer strands lay flat on the electrode surface. The pzc value of the Apt/AuED-MEAs was 0.25 V and therefore more cathodic than the lower limit of the potential pulse. Consequently, the electrode remained positively charged during the entire pulse cycle, attenuating the ion stirring effect, blocking the electrode surface with the initially immobilized aptamer strands, and impeding the accessibility of the new aptamers. Further decreasing the lower potential (pulse profile +0.6/-0.1 V) led to a significant decrease of the immobilization yield for the aptamers (Fig. 3a). The decreased aptamer yield might be due to a more pronounced potential drop at higher applied potentials, resulting in a lower averaged potential value (Kaiser and Rant, 2010). Moreover, the electrostatic repulsion between the electrode and aptamer prevents the strand-binding at high negative potentials. Consequently, the ionic flow and stirring effect were reduced during aptamer immobilization. To evaluate the impact of oxygen on the immobilization efficiency due to hydrogen peroxide formation at cathodic potentials (−0.1 V), the deposition process was conducted under an argon atmosphere. The results show that the obtained surface coverage remains unchanged with (+) and without (−) argon purging, suggesting minimal effects of oxygen during the deposition step (Fig. S5a). Notably, the reduced variability in surface coverage observed under argon protection suggest an improved immobilization reproducibility, enhancing the stability of the PA immobilization method.

In addition, the pulse duration at each given potential had a significant impact on the immobilization efficiency. On one hand, the pulse duration must be long enough to allow an entire aptamer molecule to reach the electrode surface and form an Au-S bond, regardless of the initial strand orientation. On the other hand, shorter pulse durations increase the number of stirring cycles during the overall immobilization process, which can draw a larger amount of aptamer molecules from the bulk solution during the PA process (Jambrec et al., 2015). We demonstrate this by using the same potential profile (+0.6/+0.1 V) while only varying the pulse duration from 0.1 s to 30 s (Fig. 3b). The highest aptamer coverage was observed for a duration of 1 s, that is sufficiently long for the complete strands to be pulled down, yet short enough to allow for a high number of potential-pulse cycles. Noteworthy, increasing the number of duty cycles does not enhance the surface coverage of aptamers once a stable surface density is achieved. Apparently, the polarization to negative potential repels aptamer strands, preventing further adsorption. Therefore, increasing the duty cycle could not enhance the surface coverage beyond a steady state but improve the reproducibility of the PA deposition (Fig. S5b). Consequently, the PA method with a pulse profile of (+0.6/+0.1 V, 1 s duration) was employed for aptasensor fabrication on the AuED-MEAs.

Since the signal gain of the aptasensor arises from the conformational rearrangement of the immobilized aptamers on the AuED-MEAs, the density of the aptamer molecules tethered to the surface needs to be optimized for optimal sensor performance. Different aptamer densities can be achieved by varying the overall PA method duration. As the PA immobilization time increases, the number of attached aptamers also increases. Their sensing performance was tested for the detection of 10 nM ST, Fig. 3c. The response of the aptasensor increased rapidly and then decreased slowly for times longer than 5 min. An aptasensor with a low receptor density may suffer from insufficient binding events, while with excessively dense strands experiences high steric hindrance and limited aptamer folding space, thereby decreasing target binding effectiveness (Kjällman et al., 2008). Consequently, a PA method with a 5-min processing time was selected for E-AB sensor fabrication on AuED-MEAs.

For the optimal pulse profile, a surface aptamer coverage of $1.43 \pm 0.37 \times 10^{13}$ molecules/cm^2 was obtained, which is not statistically different from the commonly used drop-casting method ($1.22 \pm 0.44 \times 10^{13}$ molecules/cm^2) (Fig. 3d). The drop-casting method relies on the diffusion of aptamer from the bulk solution to the electrode surface, which is a slow process (overnight incubation) for low concentrations (less than 1 μM). The proposed PA method overcomes this limitation and significantly accelerates the immobilization process by using pulse-type modulation, achieving the desired surface aptamer coverage within 5 min. The sensors prepared by the PA immobilization method yield a higher signal gain towards the same concentration of analyte, which can be attributed to the improved orientation of aptamers achieved through the PA method. Furthermore, the error margin reduced considerably, indicating a higher repeatability of the PA immobilization in comparison to the drop-casting method (Fig. S5c) (Schreiber, 2000). Moreover, the *I-t* curve recorded during the PA deposition process shows a comparatively fast decrease in electrode current, reaching a plateau after several minutes (Fig. 3e). A time constant (τ) of 55.8 ± 5.9 s was obtained, implying a fast kinetics of aptamers immobilization during the PA process. It is noteworthy that the time constant for thiol-PEG immobilization was 29.9 ± 3.9 s. The faster kinetics of the latter can be explained by the reduced number of binding sites on the electrode after aptamer occupation. Other reasons can be excluded, as the molecular weight of the aptamer and the thiol-PEG were in the same range and the aptamer carries many charged groups facilitating electrostatic attraction while the transport of PEG is mainly driven by the ionic flow. Additionally, corresponding EIS measurements were used to characterize the change in electron transfer resistance (R_{et}) during the process of receptor layer formation (Fig. S6). The immobilization of aptamers resulted in a significant increase in R_{et} due to repulsion between the negatively charged aptamer and the redox probes. A further increase in the R_{et} indicated the successful thiol-PEG immobilization by the PA process. These results demonstrate that PA deposition is an effective and versatile method for developing aptasensors on MEA chips.

3.2. Analytical performance of proposed aptasensor

To investigate the analytical performance of the proposed sensor, the calibration curve was determined through ACV measurements by sequentially adding various concentrations of ST. A 15-min incubation time of ST was chosen as the optimal duration, representing the best compromise between short assay times and high sensor signals (Fig. 3f). Noteworthy, the faraday currents recorded for the developed aptasensors result from redox probes that are attached to the aptamer molecules. Upon conformational rearrangements of the aptamers due to target binding, the distance of the redox tag relative to the electrode surface changes. The ability of aptamers to adopt diverse three-dimensional conformations is intrinsically determined by their nucleotide sequence and the resulting structural flexibility. Specific sequences dictate the formation of distinct structural motifs. Upon target recognition, aptamers undergo conformational rearrangements. The magnitude and pathway of these structural transitions vary depending on the aptamer's sequence, motif type, and interaction with the analyte, resulting in differences in the distance between the redox tag and the electrode surface, generating variations in signal gain among the different sensors. As a result, 'signal-on' characteristics are observed for Glu showing increasing currents for increasing concentration and

'signal-off' responses for DA and ST with currents decreasing for increasing concentrations. Furthermore, it should be noted that the measured electrochemical signal can be modeled by an adsorption isotherm describing the NTs concentration dependent occupation of the adsorption sites, represented by the surface tethered aptamer molecules. Here, a Langmuir-Freundlich model was used to take the inhomogeneity among the adsorption sites into account (Ricci et al., 2016). The apparent K_d values were determined from electrochemical assays by fitting the experimental data to the binding model. The calculated values are 2.7 nM for ST aptamer, 1.8 nM for Glu aptamer and 49.6 μM for DA aptamer. The differences between these values and those reported in solution-phase studies can be attributed among others to the altered folding and binding dynamics in a confined 2D space at the electrode interface compared to those in a 3D environment in bulk solution. Moreover, the aptamer monolayer stability was investigated by performing consecutive ACV scans without adding the target (Fig. S7). During continuous ACV recording, only minimal changes in the peak current were observed for all three sensors, suggesting that the monolayer stability is adequate under our experimental conditions and the main redox peak of the molecular beacon remained stable across multiple measurements, indicating that the aptamer monolayer is sufficiently packed for reliable target detection.

For ST sensor, the peak current of the ACV curve decreased as the concentration of the target increased (Fig. 4a). Given the assumption that the signal gain is proportional to the amount of bounded ST, the signal gain is plotted versus the logarithm of analyte concentrations. This can be fitted by the above mentioned Langmuir-Freundlich model (Fig. 4d). A semi-logarithmic relationship was found from 0.1 nM to 1000 nM, following the equation: Signal gain (%) = 12.11 lg C + 33.23, with a correlation coefficient of 0.99 (Fig. 4g). The limit of detection (LOD) was calculated to be 8 pM, defined as the mean of the blank signal plus three times the standard deviation.

Similarly, E-AB sensors for the detection of Glu and DA were fabricated using the PA deposition method and validated for various concentrations of the respective target analytes. The ACV signals were recorded after 10 min and 15 min of incubation for DA and Glu, respectively, in accordance with the optimized signal-time dependence (Fig. S8). For the Glu sensor, the peak current of the ACV curve increased as the concentration of the target increasing (Fig. 4b). Again, semi-logarithmic relationship was found from 0.1 nM to 10 μM, following the relation: Signal gain (%) = 25.24 lg C + 62.42, with a correlation coefficient of 0.99 (Fig. 4e) and the LOD was calculated to be 32 pM (Fig. 4h). The DA sensor showed a decrease in the ACV peak current as the concentration of DA increased (Fig. 4c). The detection range covered

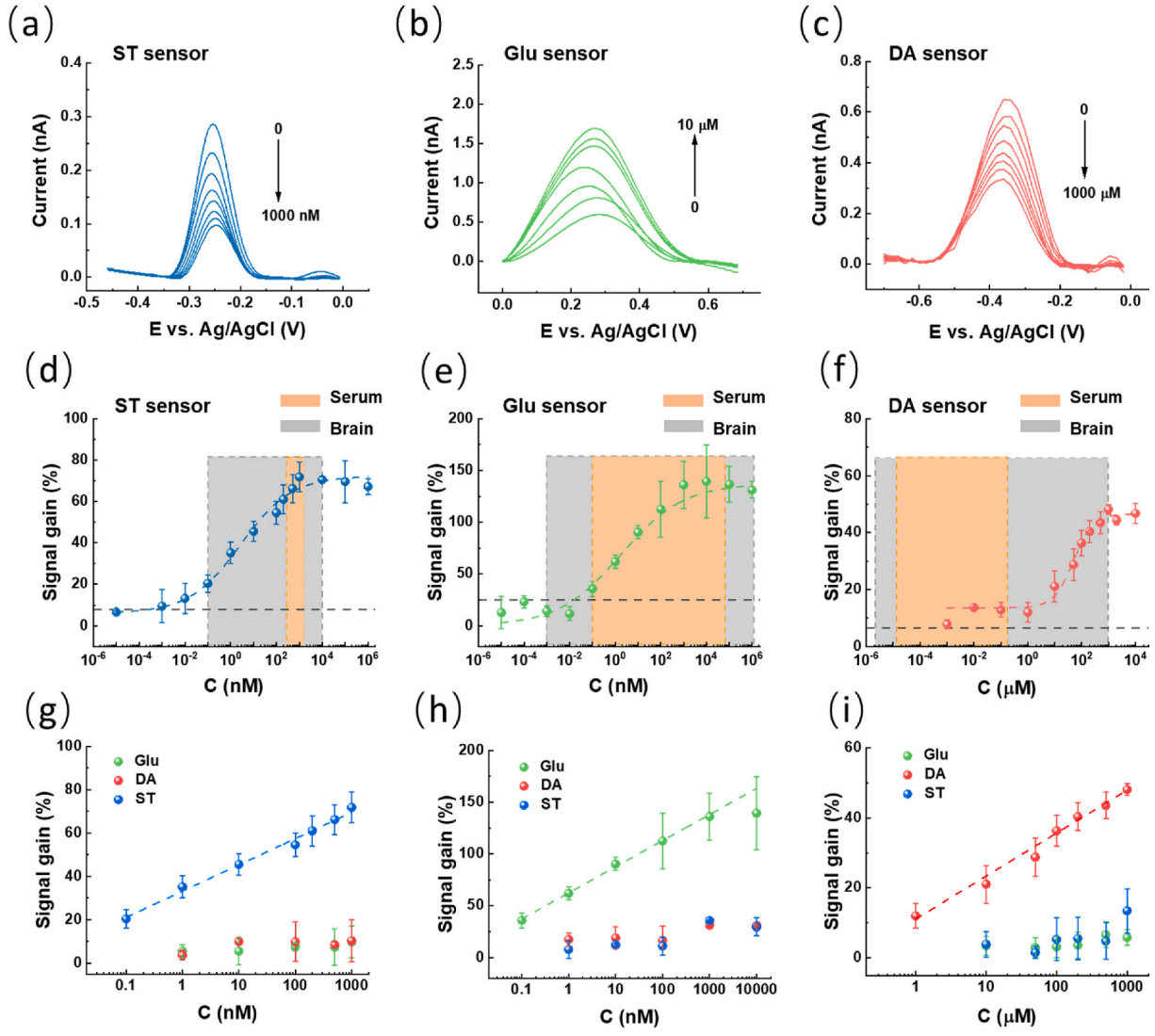

Fig. 4. ACV response of the three electrochemical aptasensors after incubation in different concentrations of the three analytes: (a) ST, (b) Glu, and (c) DA. (d) to (f) show the corresponding signal gain plotted versus the logarithm of analyte concentrations (Horizontal dashed lines in panels d–f represent the LoD threshold (blank signal ± 3SD)). (g) to (i) show the dynamic detection ranges of the sensors with linear relationship in a semi-logarithmic presentation.

a concentration window lasting from 1 μM to 1000 μM while the calibration equation was Signal gain (%) = 12.27 lg C + 11.08 with a correlation coefficient of 0.99 (Fig. 4f) and a LOD of 0.41 μM (Fig. 4i). To enable direct comparison across different aptamer channels, raw electrochemical signal gains were normalized to a relative scale based on each channel's dynamic range (Fig. S9). This strategy not only compensates for intrinsic differences in aptamer conformational behavior but also enhances the clinical utility of the sensor array by providing consistent and interpretable outputs across multiple sensing channels. The proposed E-AB sensor array demonstrates effective sensing performance across a broad range of physiologically relevant neurotransmitter concentrations found in the brain and, to a lesser extent, in serum (Fig. 4d–f). Compared to other previously reported methods, our sensor array exhibited promising sensitivity for the NTs analysis (Table S1).

3.3. Simultaneous detection of multiple NTs

To enable the simultaneous monitoring of ST, Glu, and DA on a single MEAs chip, their specific aptamers were site-selectively immobilized on different channels of the same chip using the PA deposition method. Since all the MEAs channels were exposed to the solution containing the thiol molecules after first aptamer immobilization, a regeneration of the unmodified electrodes was crucial for establishing a multi-aptamer sensor platform. This was achieved by electrodesorption of the thiol SAM from the electrode surface using CV scanning in 0.5M NaOH (Fig. S10a). A typical cathodic current peak was observed at −1.1V, indicating the desorption of the thiol monolayer from the gold surface (Lee and Lennox, 2007). After cleaning, a full regeneration of the ESA of the AuED-MEAs was obtained as demonstrated by the similarity of the oxidation/reduction cycles of the fresh electrode and the same electrode after thiol SAM deposition and electrodesorption (Fig. S10b). The reactivated electrode was subsequently used for Glu aptasensor fabrication by performing the PA process in a solution containing Glu-aptamers. For the development of the DA aptasensor, a similar regeneration and immobilization procedure was performed on another set of specific microelectrodes on the same chip. This process resulted in a triple aptamer-functionalized AuED-MEAs chip. Notably, the regeneration procedure did not impair the binding capability of the aptamers, even though they were exposed to corrosive NaOH conditions. The high chemical robustness of aptamers allows them to remain unaltered under harsh conditions.

One major challenge for multiplexed detection on a single chip is crosstalk and interference between the different adjacent aptasensors. To demonstrate the absence of interference during the simultaneous detection of the three analytes, the triple aptamer-functionalized AuED-MEA chips were tested for the detection of ST, Glu, and DA in the same sample solution. In the absence of all analytes, a well-defined electrochemical MB peak at −0.25 V was observed in the PBS buffer for the ST aptasensor (Fig. 5a). For the channels with the Glu and DA aptasensor, characteristic peaks for Fc and AQ at 0.3 V and −0.4 V were detected, respectively (Fig. 5b and c). This finding confirms the precise immobilization of the respective aptamers on the spatially separated electrodes of the MEAs chip, which prevents cross contaminations between the aptamer molecules. The addition of Glu and DA caused only a small alteration of the current for the ST aptasensor channel, whereas a target-concentration-dependent decrease in current was observed upon the addition of ST. Similarly, the Glu aptasensor and DA aptasensor exhibited target concentration-dependent signal gains only in the presence of their respective targets, with minimal interference from the other analytes. The high selectivity of the proposed aptasensors was further validated by testing against individual analog molecules (Fig. 5d). The developed E-AB sensors displayed comparably low signal variations for interfering molecules, while a distinct signal increase was observed for the desired target, even when its concentration was two orders of magnitude lower than that of the analog molecules. Marginal crosstalk between the analyte signals was observed which can be

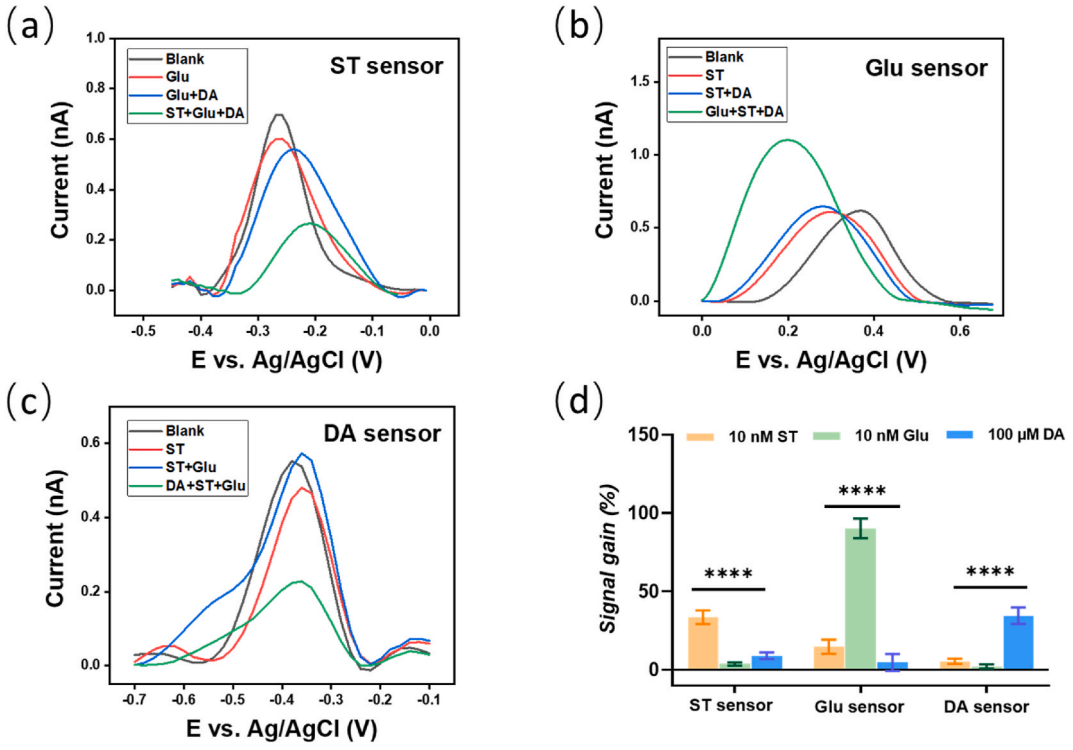

Fig. 5. Simultaneous detection of multiple NTs from different aptamer-modified AuED electrodes of the same MEA chip. ACV responses of (a) ST-aptasensor, (b) Glu-aptasensor, and (c) DA-aptasensor for addition of three analytes (ST: 10 nM, Glu: 10 nM, DA: 100 μM) in PBS solution (137 mM NaCl, 2.7 mM KCl, 10 mM Na_2HPO_4, 1.8 mM NaH_2PO_4, 2 mM $MgCl_2$, pH 7.4). (d) The selectivity of developed E-AB sensors with minimal crosstalk and interferences distinguishing the desired target analyte molecules (****$p < 0.001$).

attributed to the high accuracy of the aptamer immobilization and the specificity of the aptamer receptors towards their target analytes. Noteworthy, the signal did not increase proportionally with increasing non-target concentrations, confirming that non-specific binding events from interfering species had negligible effects (Fig. 4g–i). Consequently, this aptasensor can distinguish the target analyte from other NTs and the non-target signals remained significantly lower than that of the specific target over a wide concertation range. Overall, these studies demonstrate that our triple aptasensor exhibits high accuracy and feasibility for the simultaneous detection of ST, Glu, and DA in different channels on the same chip, with minimal crosstalk and interference.

3.4. Real sample test

To evaluate the sensing performance of the proposed aptasensors in a complex environment, all three analytes were tested in artificial cerebrospinal fluid (aCSF) using the standard addition method. Our data showed promising recovery rates ranging from 101.1 % to 111.0 %, with relative standard deviations (RSD) from 3.6 % to 19.4 %. This indicates that the PEG-blocked aptasensor has high reliability in brain-like microenvironments (Table S2).

To further assess the detection of NTs in real samples, human serum diluted to 50 % was analyzed using the developed sensors. A variety of clinically relevant target concentrations, including low, medium, and high levels, were spiked in serum samples and compared with the results obtained from PBS samples. The recovery rates for real samples were 109.1 %–125.4 %, 97.3 %–116.8 % and 106.2 %–117.0 % for ST, Glu, and DA, respectively, indicating the feasibility of detecting the targets in complex biological matrices (Fig. 6a–c). The tested concentrations are within the reported ranges associated with Alzheimer's and Parkinson's diseases, demonstrating the potential of our sensor for neurological diagnostics (Arumugasamy et al., 2020). Moreover, the calculated LOD values of the sensors in serum were 9.2 pM for ST, 51.5 pM for Glu, and 0.84 μM for DA (Fig. S11). These results are comparable to those obtained in buffer conditions, further supporting the practical applicability of our system for clinical analysis. Additionally, to validate the minimal crosstalk and interference, the signal gain towards non-specific analytes were measured in 50 % serum for each aptamer-functionalized electrode. The results support the high specificity and minimal biofouling of the proposed sensor in complex biological matrices (Fig. 6d). The antifouling property of the aptasensor originates from the formation of a hydrophilic thiol-PEG monolayer, which significantly prevents nonspecific protein adsorption onto the sensing surface (Figueroa-Miranda et al., 2020). These findings clearly demonstrate that the constructed aptasensor can achieve the performance required to support disease diagnostics and *in vitro* or *in vivo* recordings of NT release in complex biomatrices.

4. Conclusions

In this study, a multiplex aptamer-functionalized microelectrode array chip was developed for the simultaneous detection of NTs. A chronoamperometric gold plating technique was employed to electrodeposit nanogold on the microelectrodes, applying a potential of 0.6 V (Ag/AgCl) for a period of 7 min. This resulted in an optimal balance between large active surface areas and high nanostructure stability. The resulting three-dimensional nanostructures resulted in a notable increase in receptor load and a considerable reduction in electron transfer resistance. A potential-pulse assisted (PA) deposition method was developed to enable site-selective immobilization of multiple aptamers on individual electrodes of a single MEA chip. Remarkably, the PA approach achieved surface coverages comparable to conventional drop-casting methods, yet reduced the processing time from several hours to only 5 min, representing a significant advance in sensor fabrication

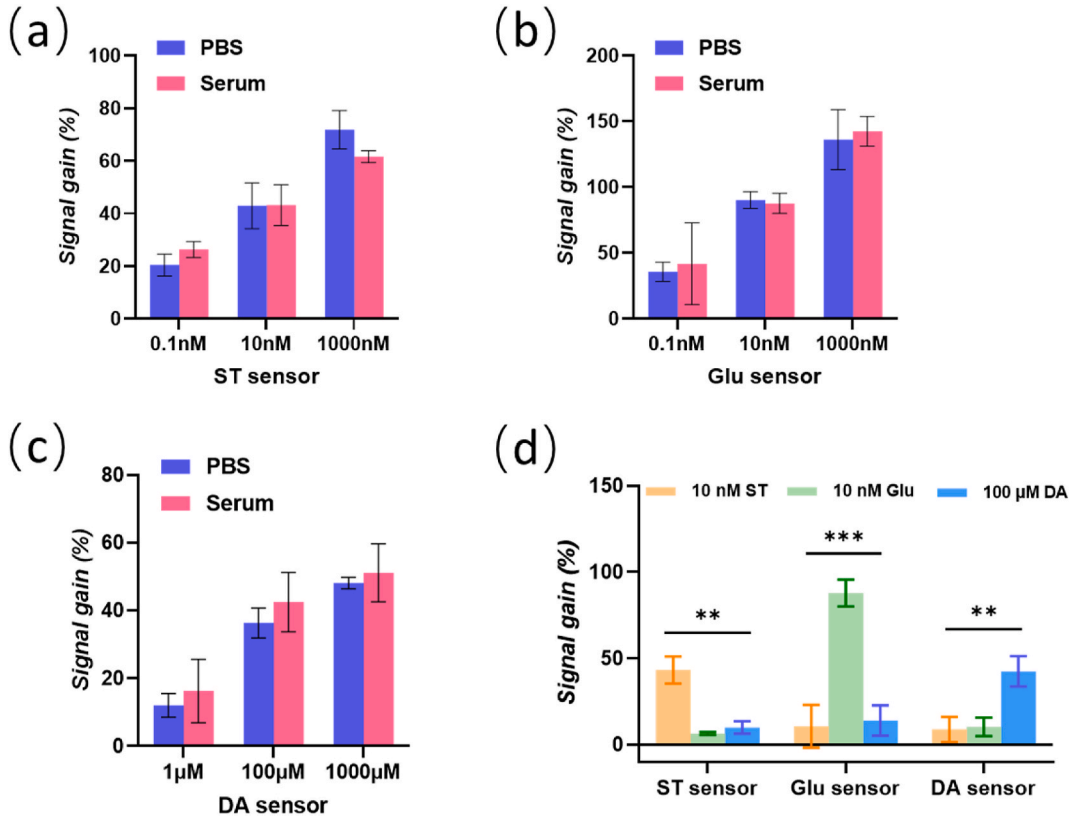

Fig. 6. (a)–(c) Recoveries in 50 % human serum determined by the standard addition method with the addition of different concentrations of the NTs. (d) The developed E-AB sensors showed minimal crosstalk and interferences in serum sample (**p < 0.01, ***p < 0.005).

efficiency. This was achieved through the optimization of the pulse profile to +0.6/+0.1 V and a 1-s pulse duration. The PA technique was utilized for the deposition of the thiol-PEG too. The rapid immobilization kinetics of the pulsed microelectrodes, in comparison to those under open circuit conditions, in conjunction with an electrochemical electrode regeneration method applied to the latter, facilitated the site-selective immobilization of aptamers. The E-AB sensors, which were developed as part of this study, exhibited a wide linear range (as presented in semi-logarithmic form) and low LOD of 8 pM for ST, 32 pM for Glu, and 0.41 μM for DA. Moreover, the possibility of concurrent monitoring of multiple NTs on a single chip with minimal cross-talk and interference was demonstrated. The utilization of a multielectrode array enables redundant detection of the analytes from multiple recording sites of the same sample, allowing an averaging of the recording results, which improves assay accuracy, avoids assay repetitions, provides synchronized sensor responses, minimizes sample consumption, reduces assay time, and enhances overall testing efficiency. The utilization of thiol-PEG backfill molecules effectively suppressed non-specific adsorption, thereby enabling the detection of analytes in complex samples with high reproducibility. Notably, the developed E-AB sensors maintained comparable detection limits even in serum, thereby demonstrating their robustness in complex biological environments and underscoring their potential utility for clinical analysis. Overall, the proposed biosensing platform demonstrates considerable potential for the study of the co-release of multiple NTs in neuroscience, exhibiting high sensitivity and specificity. In the future, it is intended to implement this sensor in *in vitro* and *in vivo* experiments where spatial-temporal variations of the release of various NTs in nervous tissue should be studied, which is illusive with the current technology. The sensor presented in this work is a critical step towards the realization of such multianalyte sensor, which will facilitate the investigation of NTs projections within the brain, a fundamental for complex cognitive functions. Furthermore, given the sensor's performance, versatility, and rapid preparation, we envisage this method being extended for the determination of other biomarkers, as it meets the requirements of point-of-care testing and clinical diagnostics.

CRediT authorship contribution statement

Ziheng Hu: Writing – original draft, Methodology, Investigation, Formal analysis, Data curation. **Ruifeng Zhu:** Methodology, Investigation, Data curation. **Gabriela Figueroa-Miranda:** Methodology, Formal analysis. **Lingyan Feng:** Writing – review & editing, Supervision. **Andreas Offenhäusser:** Supervision, Resources. **Dirk Mayer:** Writing – review & editing, Supervision, Conceptualization.

Declaration of competing interest

The authors declare that they have no known competing financial interests or personal relationships that could have appeared to influence the work reported in this paper.

Acknowledgement

Ziheng Hu gratefully acknowledges financial support from the China Scholarship Council (No. 202006890001). The authors are grateful to Marko Banzet for the fabrication of the MEA chips.

Appendix A. Supplementary data

Supplementary data to this article can be found online at https://doi.org/10.1016/j.bios.2025.117992.

Data availability

Data will be made available on request.

References

Arumugasamy, S.K., Chellasamy, G., Gopi, S., Govindaraju, S., Yun, K., 2020. TrAC, Trends Anal. Chem. 123, 115766.
Bucher, E.S., Wightman, R.M., 2015. Annu. Rev. Anal. Chem. 8, 239–261.
Downs, A.M., Plaxco, K.W., 2022. ACS Sens. 7, 2823–2832.
Fan, J., Tang, Y., Yang, W., Yu, Y., 2020. J. Mater. Chem. B 8, 7501–7510.
Feng, L., Lyu, Z., Offenhäusser, A., Mayer, D., 2016. Eng. Life Sci. 16, 550–559.
Figueroa-Miranda, G., Chen, S., Neis, M., Zhou, L., Zhang, Y., Lo, Y., Tanner, J.A., Kreidenweiss, A., Offenhäusser, A., Mayer, D., 2021. Sensor. Actuator. B Chem. 349, 130812.
Figueroa-Miranda, G., Wu, C., Zhang, Y., Nörbel, L., Lo, Y., Tanner, J.A., Elling, L., Offenhäusser, A., Mayer, D., 2020. Bioelectrochemistry 136, 107589.
Gao, Z., Wu, G., Song, Y., Li, H., Zhang, Y., Schneider, M.J., Qiang, Y., Kaszas, J., Weng, Z., Sun, H., Huey, B.D., Lai, R.Y., Zhang, Y., 2022. Anal. Chem. 94, 8605–8617.
Ge, C., Liao, J., Yu, W., Gu, N., 2003. Biosens. Bioelectron. 18, 53–58.
Gibson, J.S., Mendes, P.M., 2021. ChemPhysChem 22, 684–692.
Hansen, J.A., Wang, J., Kawde, A.-N., Xiang, Y., Gothelf, K.V., Collins, G., 2006. J. Am. Chem. Soc. 128, 2228–2229.
Hu, Z., Li, Y., Figueroa-Miranda, G., Musall, S., Li, H., Martínez-Roque, M.A., Hu, Q., Feng, L., Mayer, D., Offenhäusser, A., 2023a. TrAC, Trends Anal. Chem. 162, 117021.
Hu, Z., Zhu, R., Figueroa-Miranda, G., Zhou, L., Feng, L., Offenhäusser, A., Mayer, D., 2023b. Biosensors 13, 881.
Jambrec, D., Gebala, M., 2022. Chemelectrochem 9, e202101415.
Jambrec, D., Gebala, M., La Mantia, F., Schuhmann, W., 2015. Angew. Chem. Int. Ed. 54, 15064–15068.
Jambrec, D., Kayran, Y.U., Schuhmann, W., 2019. Electroanalysis 31, 1943–1951.
Kaiser, W., Rant, U., 2010. J. Am. Chem. Soc. 132, 7935–7945.
Kjällman, T.H.M., Peng, H., Soeller, C., Travas-Sejdic, J., 2008. Anal. Chem. 80, 9460–9466.
Lee, L.Y.S., Lennox, R.B., 2007. Langmuir 23, 292–296.
Li, F., Guo, Y., Wang, X., Sun, X., 2018. Biosens. Bioelectron. 115, 7–13.
Liu, X., Hou, Y., Chen, S., Liu, J., 2021. Biosens. Bioelectron. 173, 112798.
Ma, C., Liu, H., Zhang, L., Li, H., Yan, M., Song, X., Yu, J., 2018. Biosens. Bioelectron. 99, 8–13.
Ma, L., Zhao, T., Zhang, P., Liu, M., Shi, H., Kang, W., 2020. Anal. Biochem. 593, 113594.
Moraldo, C., Vuille-dit-Bille, E., Shkodra, B., Kloter, T., Nakatsuka, N., 2022. J. Neurosci. Methods 365, 109386.
Munge, B.S., Stracensky, T., Gamez, K., DiBiase, D., Rusling, J.F., 2016. Electroanalysis 28, 2644–2658.
Nakatsuka, N., Yang, K.-A., Abendroth, J.M., Cheung, K.M., Xu, X., Yang, H., Zhao, C., Zhu, B., Rim, Y.S., Yang, Y., Weiss, P.S., Stojanović, M.N., Andrews, A.M., 2018. Science 362, 319–324.
Negahdary, M., Angnes, L., 2022. Biomater. Adv. 135, 112689.
Pradhan, T., Jung, H.S., Jang, J.H., Kim, T.W., Kang, C., Kim, J.S., 2014. Chem. Soc. Rev. 43, 4684–4713.
Ricci, F., Vallée-Bélisle, A., Simon, A.J., Porchetta, A., Plaxco, K.W., 2016. Acc. Chem. Res. 49, 1884–1892.
Schreiber, F., 2000. Prog. Surf. Sci. 65, 151–257.
Sen, D., Lazenby, R.A., 2024. Anal. Sens. 4, e202300047.
Sharafeldin, M., Rusling, J.F., 2023. Curr. Opin. Electrochem. 39, 101256.
Shen, Z., Ni, S., Yang, W., Sun, W., Yang, G., Liu, G., 2021. Sensor. Actuator. B Chem. 336, 129747.
Soleymani, L., Fang, Z., Sargent, E.H., Kelley, S.O., 2009. Nat. Nanotechnol. 4, 844–848.
Song, W., Li, H., Liang, H., Qiang, W., Xu, D., 2014. Anal. Chem. 86, 2775–2783.
Teleanu, R.I., Niculescu, A.-G., Roza, E., Vladâcenco, O., Grumezescu, A.M., Teleanu, D. M., 2022. Int. J. Mol. Sci. 23, 5954.
Ter-Ovanessian, B., Alemany-Dumont, C., Normand, B., 2014. J. Appl. Electrochem. 44, 399–410.
Timilsina, S.S., Jolly, P., Durr, N., Yafia, M., Ingber, D.E., 2021. Acc. Chem. Res. 54, 3529–3539.
Tomić, S., Babić, S.D., Vuletić, T., Krča, S., Ivanković, D., Griparić, L., Podgornik, R., 2007. Phys. Rev. 75, 021905.
Torrente-Rodríguez, R.M., Lukas, H., Tu, J., Min, J., Yang, Y., Xu, C., Rossiter, H.B., Gao, W., 2020. Matter 3, 1981–1998.
Venton, B.J., Cao, Q., 2020. Analyst 145, 1158–1168.
Veselinovic, J., Li, Z., Daggumati, P., Seker, E., 2018. Electrically guided DNA immobilization and multiplexed DNA detection with nanoporous gold electrodes. Nanomaterials 8 (5), 351.
Wojnicz, A., Avendaño Ortiz, J., Casas, A.I., Freitas, A.E., G. López, M., Ruiz-Nuño, A., 2016. Clin. Chim. Acta 453, 174–181.
Wu, C., Barkova, D., Komarova, N., Offenhäusser, A., Andrianova, M., Hu, Z., Kuznetsov, A., Mayer, D., 2022. Anal. Bioanal. Chem. 414, 1609–1622.
Wu, C., Offenhäusser, A., Mayer, D., 2020. Phys. Status Solidi 217, 1900925.
Yu, H., Alkhamis, O., Canoura, J., Liu, Y., Xiao, Y., 2021. Angew. Chem. Int. Ed. 60, 16800–16823.
Zhang, Y., Figueroa-Miranda, G., Wu, C., Willbold, D., Offenhäusser, A., Mayer, D., 2020. Nanoscale 12, 16501–16513.
Zhang, Y., Jiang, N., Yetisen, A.K., 2021. Biosens. Bioelectron. 189, 113351.
Zhou, L., Figueroa-Miranda, G., Chen, S., Neis, M., Hu, Z., Zhu, R., Li, Y., Prömpers, M., Offenhäusser, A., Mayer, D., 2023. Sensor. Actuator. B Chem. 386, 133730.